5-10-2006

Correcting Unwanted Amplitude Modulation in Electro-optic Modulators

Kevin Doyle
Trinity University

Correcting Unwanted Amplitude Modulation in Electro-optic Modulators

Kevin Doyle

A DEPARTMENT HONORS THESIS SUBMITTED TO THE
DEPARTMENT OF PHYSICS & ASTRONOMY AT TRINITY UNIVERSITY
IN PARTIAL FULFILLMENT OF THE REQUIREMENTS FOR GRADUATION
WITH DEPARTMENTAL HONORS

4/19/2006

_____ _____

THESIS ADVISOR DEPARTMENT CHAIR

_____

ASSOCIATE VICE PRESIDENT FOR ACADEMIC AFFAIRS,
CURRICULUM AND STUDENT ISSUES

Acknowledgements

I would like to acknowledge all the members of the Trinity University Department of Physics & Astronomy for encouraging me to complete an Honors thesis. I would also like to thank my advisor Dr. Ugolini for his guidance, expertise, and above all, his patience.

Table of Contents

Abstract

The Laser Interferometer Gravitational Wave Observatory (LIGO) is designed to detect disturbances in spacetime created by the motion of large masses, referred to as gravitational waves. The effects of gravitational waves seen on Earth are very small; waves arriving at Earth are only expected to disturb spacetime by a factor of 10^{-21}, thus LIGO must be extremely sensitive to detect their effects. In order to increase LIGO's sensitivity, the lengths of LIGO's arm cavities must be carefully controlled and sensed. One component of a subsystem used to attain such control is an electro-optic modulator. Also known as a Pockels cell, an electro-optic modulator consists of a crystal whose indices of refraction vary with an applied voltage. Depending on its orientation, a Pockels cell can be used to introduce either phase modulation or amplitude modulation in polarized light. LIGO uses a Pockels cell to modulate the phase of an infrared laser in this manner, but over time unwanted amplitude modulation has been observed as well. Such amplitude modulation produces noise that must be eliminated. This amplitude modulation most likely comes from drifting alignment between the Pockels cell and the polarization angle of the laser, and so a feedback control system was designed to correct it. Two possible actuators were considered for the feedback control system, a Faraday rotator and a picomotor. The Faraday rotator used in this experiment proved ineffective in correcting the amplitude modulation because it was unable to rotate the polarization angle of the laser far enough to bring it back in alignment with the Pockels cell. A different Faraday rotator capable of greater rotation could still work, but such a Faraday rotator may prove unfeasible when actuating LIGO's Pockels cell. However, the picomotor proved much more effective, correcting the alignment and thus rectifying the problem in a matter of minutes. Having successfully tested this feedback control system with a picomotor as the actuator, a similar feedback control system can be created for LIGO, bringing the apparatus one step closer to its ultimate goal of detecting gravitational waves.

Chapter 1: Gravitational Waves & LIGO

1.1 Gravitational Waves

First postulated by Albert Einstein in his General Theory of Relativity, gravitational waves are disturbances that alternately shrink and stretch the curvature of spacetime. These waves are produced by the motion of large masses, much the same way that electromagnetic waves are produced by moving charges (1). Just as the development of radio astronomy revealed new phenomena to study such as pulsars and quasars, so too could a thorough understanding of gravitational waves open up new observations of the universe. Astronomy based on gravitational waves could reveal information about the coalescence of pairs of neutron stars, the creation of neutron stars in supernovae, the swallowing of neutron stars by black holes, and a whole host of other phenomena yet to be discovered (2).

Unfortunately, gravitational waves have yet to be observed directly. They remained purely theoretical until 1974, with the discovery of a binary pulsar by Russell A. Hulse and Joseph H. Taylor. Using the General Theory of Relativity, Hulse and Taylor predicted that the binary pulsar would lose energy through the emission of gravitational waves, and that this energy loss would alter the orbital period at a specific rate. Their observations of the system's orbital period over time agreed with this prediction, marking the first experimental evidence of the existence of gravitational waves (1). However, because the strength of a gravitational wave decreases proportionally with the square of the distance from the source, by the time the waves arrive at Earth their effects are too weak to detect. The strongest source of gravitational waves seen on Earth is a black hole/black hole inspiral, i.e. a group of black holes orbiting one another and thus emitting gravitational waves in the same manner as the binary pulsar studied by Hulse and Taylor. Gravitational waves from these inspirals, which are most likely located in the Virgo cluster of galaxies 20 megaparsecs away, will only generate a strain of around 10^{-21} on Earth; currently, such strains are too small to detect (3).

Thus in order to detect gravitational waves on Earth despite their miniscule effect, a number of facilities have been created to measure the effects of gravitational waves and observe them directly. One such facility is the Laser Interferometer Gravitational Wave Observatory, or LIGO, which consists of two sites in Livingston, Louisiana and Hanford Washington. Other facilities include GEO in Germany, VIRGO in Italy, TAMA in Japan, and ACIGA in Australia (4). Working together, these facilities hope to collaborate on different methods and verify each other's findings, eventually allowing astrophysicists to observe gravitational waves on Earth directly.

1.2 LIGO

LIGO is a 2.5 mile long Michelson interferometer, a device which can measure very small changes in length with great precision (2). A Michelson interferometer consists of two intersecting perpendicular lever arms with mirrors at both ends, with a beam-splitter at the vertex (Fig. 1.1). A laser beam is directed into the beam splitter, which directs half

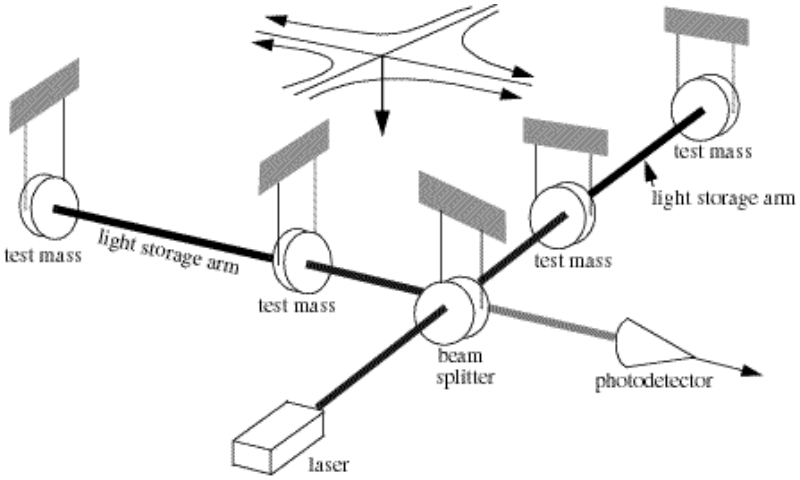

Figure 1.1: Diagram of LIGO (5)

the beam down one lever arm and half the beam down the other. The two beam halves are reflected at the end of both lever arms by a mirror, and then sent back to be recombined and directed to a photodetector, where the two beam-halves will either interfere constructively or destructively to form an interference pattern of alternately light and dark fringes (Fig. 1.2). Small changes in the length of a lever arm can be detected by observing shifts in this interference pattern according to the equation

$$\lambda = 2\Delta d / n \qquad \textbf{(1.1)}$$

where λ is the wavelength of the laser, Δd is the change in length, and n is the number of fringes that pass through a certain point during the shift (6). Thus for a 1 micron laser, a shift of a single fringe represents a change in length 0.5 μm. While relatively sensitive, this is nowhere near sensitive enough to detect the effects of gravitational waves.

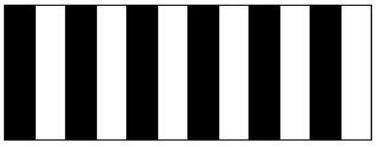

Figure 1.2: Sample interference pattern

LIGO is designed to be considerably more sensitive, so that it can detect the strain caused by gravitational waves. Because strain measures the change in length per unit length, increasing the length of LIGO's lever arms will also increase its sensitivity to strain. LIGO's lever arms are 4 kilometers (2.5 miles) in length, which makes a single fringe shift sensitive enough to detect strains as small as 10^{-10}. Unfortunately, even this is not sensitive enough, as the strain due to gravitational waves will only be about 10^{-21} (2).

To increase the sensitivity even further, both arms contain a Fabry-Perot cavity. A Fabry-Perot cavity consists of two mirrors in which the laser light bounces back and forth multiple times, "folding" the lever arm over itself and thus increasing the distance traveled by the light (6). On average the Fabry-Perot cavities increase the path-length of the beams by a factor of 300, making LIGO capable of detecting strains on the order of 10^{-13} with a single fringe shift. Therefore, in order to see a strain of 10^{-21}, LIGO would have to observe a shift of 10^{-8} of a fringe (3).

In order to minimize the random fluctuation of photons per second, or shot noise, LIGO operates by observing changes within a dark fringe. However, because the rate of change of the light is zero within dark fringes, changes in length will not affect the output enough to observe a shift of 10^{-8}. To correct for this problem, LIGO uses a technique called "heterodyning," in which sidebands are placed on the laser light with the same frequencies as the laser +/- a phase modulation frequency. As a result, the total laser beam entering the system will have an amplitude

$$\Psi = A\cos(\omega t) + B\cos[(\omega \pm \omega_m)t] \qquad \textbf{(1.2)}$$

where A is the amplitude of the original laser, B is the amplitude of the side bands, ω is the frequency of the original laser, and ω_m is the modulation frequency ($\omega_m << \omega$). The intensity of the total light entering the lever arms (I) is given by the square of equation 1.2, or

$$I = A^2\cos^2(\omega t) + AB\cos(\omega t)\cos[(\omega + \omega_m)t] + B^2\cos^2[(\omega + \omega_m)t] \qquad \textbf{(1.3)}$$

However, because signals with frequency ω are too rapid for the photodiode to detect (on the order of $3x10^4$ Hz), those signals will not register. As a result, the intensity measured by the photodiode will not include any terms with frequency ω, leaving only

$$I = A^2 + AB\cos(\omega_m t) + B^2\cos(2\omega_m t) \qquad \textbf{(1.4)}$$

Because the carrier frequency ω is resonant with the Fabry-Perot cavities and the sidebands are not, mixing this result with $\cos(\omega_m t)$ and then averaging the result produces

$$< A^2\cos(\omega_m t) + AB\cos^2(\omega_m t) + B^2\cos(\omega_m t)\cos(2\omega_m t) >= \frac{AB}{2} \qquad \textbf{(1.5)}$$

which varies linearly with the arm length precisely enough to detect a fringe shift of 10^{-8}, corresponding to the strain of a gravitational wave. The phase modulation that creates these sidebands is produced by an electro-optic modulator (7).

1.3 A Source of Noise

The electro-optic modulator used in LIGO is configured to modulate the phase of the laser beam. However, over time the electro-optic modulator also has been observed to introduce amplitude modulation, which produces noise in the final signal (8). The magnitude of this noise has also been observed to change over time, mimicking the effects of a gravitational wave. Thus such fluctuations in amplitude need to be eliminated in order to ensure that only genuine gravitational waves can produce changes in LIGO's intensity. The next chapters will examine the properties of electro-optic modulators and a potential feedback control system that will automatically correct for all amplitude modulation.

Chapter 2: Electro-optic Modulators

2.1 The Electro-optic Effect

An electro-optic modulator, or Pockels cell, consists of a crystal placed between two conducting plates used to produce an applied electric field (Fig. 2.1). By altering the electric field, the crystal's indices of refraction can be controlled, and as a result polarized light passing through the Pockels cell can experience either phase or amplitude modulation depending on its orientation with the axes of the crystal. In order to understand how phase and amplitude modulation occurs in a Pockels cell, the effect an electric field has on the crystal's indices of refraction must be determined. For any given crystal, the indices of refraction can be found using the index ellipsoid

$$\frac{x^2}{n_x^2}+\frac{y^2}{n_y^2}+\frac{z^2}{n_z^2}=1 \qquad \textbf{(2.1)}$$

where x, y, and z represent the directions of the principal dielectric axes of the crystal (in which **D** and **E** are parallel) . In cases where the index of refraction is the same for two axes and different for the third, the crystal is said to possess birefringence (9).

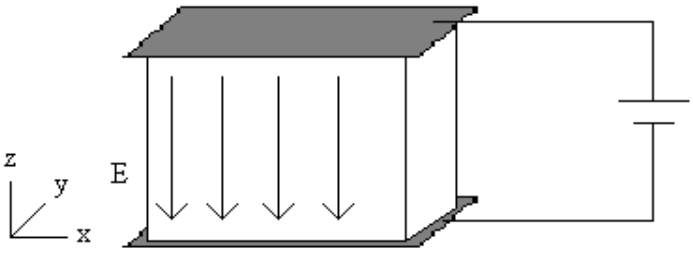

Figure 2.1: Diagram of a Pockels cell

The electro-optic effect measures the change in the indices of refraction of the crystal caused by the applied electric field. With the application of the electric field, the index ellipsoid changes to

$$\frac{x^2}{n_1^2}+\frac{y^2}{n_2^2}+\frac{z^2}{n_3^2}+2\frac{yz}{n_4^2}+2\frac{xz}{n_5^2}+2\frac{xy}{n_6^2}=1 \qquad \textbf{(2.2)}$$

where n_i represents the new index of refraction in the dielectric axis. According to the new ellipsoid, the electric field not only changes the magnitude indices of refraction for the principal dielectric axes, it introduces mixed terms to the ellipsoid as well. Thus the electric field can change the directions of the dielectric axes in addition to their magnitudes.

The new indices of refraction for an arbitrary electric field **E** (E_x, E_y, E_z), can be found using matrix equation 2.3

$$\begin{bmatrix} \Delta(\frac{1}{n_1^2}) \\ \Delta(\frac{1}{n_2^2}) \\ \Delta(\frac{1}{n_3^2}) \\ \Delta(\frac{1}{n_4^2}) \\ \Delta(\frac{1}{n_5^2}) \\ \Delta(\frac{1}{n_6^2}) \end{bmatrix} = \begin{bmatrix} r_{11} & r_{12} & r_{13} \\ r_{21} & r_{22} & r_{23} \\ r_{31} & r_{32} & r_{33} \\ r_{41} & r_{42} & r_{43} \\ r_{51} & r_{52} & r_{53} \\ r_{61} & r_{62} & r_{63} \end{bmatrix} \begin{bmatrix} E_x \\ E_y \\ E_z \end{bmatrix} \quad \textbf{(2.3)}$$

The 6x3 matrix of elements r_{ij} in equation 2.3 is called the electro-optic tensor, an intrinsic property of crystals determined by the geometry of their crystal lattice. Electro-optic tensors for most crystals can be found in crystallography textbooks. The Pockels cell used in LIGO contains the crystal lithium niobate ($LiNbO_3$), whose electro-optic tensor turns equation 2.3 into

$$\begin{bmatrix} \Delta(\frac{1}{n_1^2}) \\ \Delta(\frac{1}{n_2^2}) \\ \Delta(\frac{1}{n_3^2}) \\ \Delta(\frac{1}{n_4^2}) \\ \Delta(\frac{1}{n_5^2}) \\ \Delta(\frac{1}{n_6^2}) \end{bmatrix} = \begin{bmatrix} 4.1 & 0 & 9.6 \\ -4.1 & 0 & 9.6 \\ 0 & 0 & 30.9 \\ 0 & 32.6 & 0 \\ 32.6 & 0 & 0 \\ 0 & -4.1 & 0 \end{bmatrix} \begin{bmatrix} E_x \\ E_y \\ E_z \end{bmatrix} \quad \textbf{(2.4)}$$

where the coefficients listed in the tensor have units of 10^{-12} m/V (9). Using the rules for matrix multiplication, the new indices of refraction in equation 2.2 can be found by the equation

$$\Delta \frac{1}{n_i^2} = r_{i1}E_x + r_{i2}E_y + r_{i3}E_z \quad \textbf{(2.5)}$$

If the electric field is only applied along the z-axis, with $E_x = E_y = 0$ and $E_z = V/d$ (voltage of the plates divided by their separation), the mixed terms in equation 2.2 do not appear, and thus the direction of the dielectric axes do not change. The new indices of refraction for the principal axes, n_x, n_y, and n_z, can be calculated from equation 2.5 by

$$\frac{1}{n_x^2} = \frac{1}{n_y^2} = \frac{1}{n_o^2} + \Delta\frac{1}{n_1^2} = \frac{1}{n_o^2} + r_{13}\frac{V}{d} \quad \textbf{(2.6)}$$

and

$$\frac{1}{n_z^2} = \frac{1}{n_e^2} + \Delta\frac{1}{n_3^2} = \frac{1}{n_e^2} + r_{33}\frac{V}{d} \tag{2.7}$$

with n_o and n_e representing the ordinary and extraordinary indices of refraction of the birefringent crystal in the absence of an electric field. Solving for n_x, n_y, and n_z, and then approximating both expressions with a Taylor expansion gives

$$n_x = n_y = (\frac{1}{n_o^2} + r_{13}\frac{V}{d})^{-1/2} \approx n_o - \frac{n_o^3 r_{13}}{2}\frac{V}{d} \tag{2.8}$$

and

$$n_z = (\frac{1}{n_e^2} + r_{33}\frac{V}{d})^{-1/2} \approx n_e - \frac{n_e^3 r_{33}}{2}\frac{V}{d} \tag{2.9}$$

Both n_o and n_e can be found in any crystallography textbook. For $LiNbO_3$, n_o=2.286, n_e=2.2, r_{13}=9.6·10^{-12} m/V, and r_{33}=30.9·10^{-12} m/V (9).

2.2 Phase Modulation

Because the Pockels cell has different indices of refraction for different axes, light propagating with respect to those axes will experience different time lags. Thus when monochromatic light is directed through a linear polarizer aligned with the z-axis of the Pockels cell (Fig. 2.2), that light will experience a phase shift due to the index of refraction in that direction. We can find the change in phase shift due to an applied voltage ($\Delta\phi$) using equation 2.10

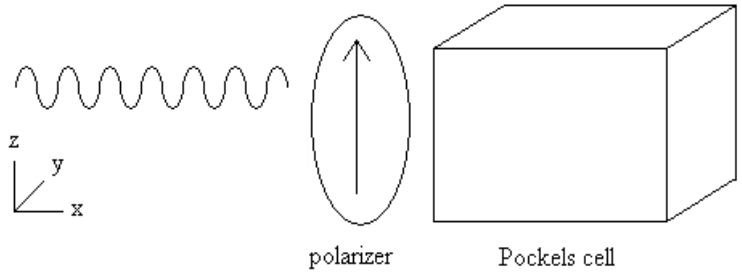

Figure 2.2: Configuration for phase modulation

$$\Delta\phi = -\frac{2\pi\ell}{\lambda}\Delta n_z = -\frac{\pi\ell n_e^3 r_{33}}{\lambda}\frac{V}{d} \tag{2.10}$$

where ℓ is the length of the Pockels cell through which the light travels.

According to this equation, the phase angle of the light depends on the voltage placed across the Pockels cell. Thus if a sinusoidal voltage $V = V_o \sin \omega t$ were applied to the Pockels cell, the phase angle of the light would likewise vary sinusoidally with time (9). In this way, phase modulation is produced by polarizing the incoming light with respect to the z-axis of the Pockels cell and applying a sinusoidal voltage (Fig. 2.3).

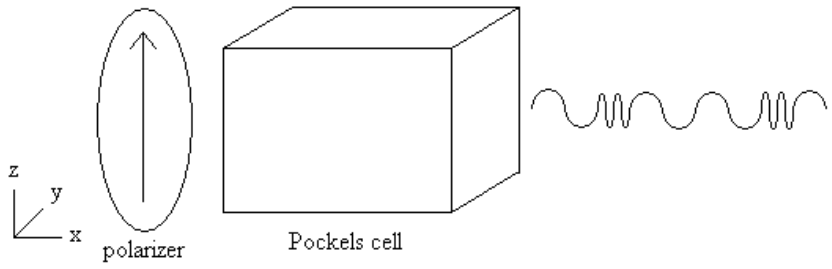

Figure 2.3: Light exits with modulated phase

2.3 Amplitude Modulation

When the incoming light is polarized at an angle θ to the z-axis of the Pockels cell (Fig. 2.4), the light will experience a time lag and thus a phase shift relative to both the z and y axes. The difference in phase shifts between the z and y axes are given by equation 2.11.

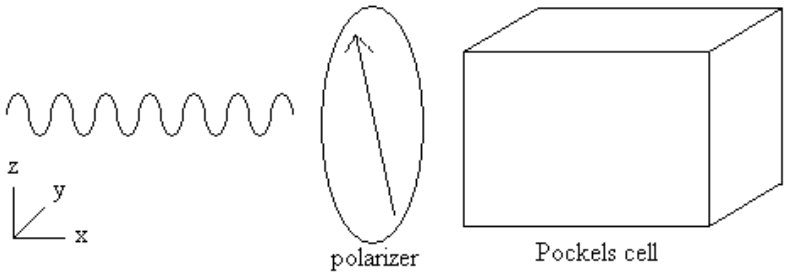

Figure 2.4: Configuration for amplitude modulation

$$\Delta\phi = \Delta\phi_z - \Delta\phi_y = -\frac{2\pi\ell}{\lambda}(n_z - n_y) = -\frac{\pi\ell}{\lambda}(n_e^3 r_{33} - n_o^3 r_{13})\frac{V}{d} \qquad \textbf{(2.11)}$$

The different phase shifts with respect to the two different axes will cause the polarization angle of the light to change with the applied voltage. Thus applying a sinusoidal voltage to the Pockels cell will cause the polarization angle to change with time after leaving the Pockels cell (Fig. 2.5).

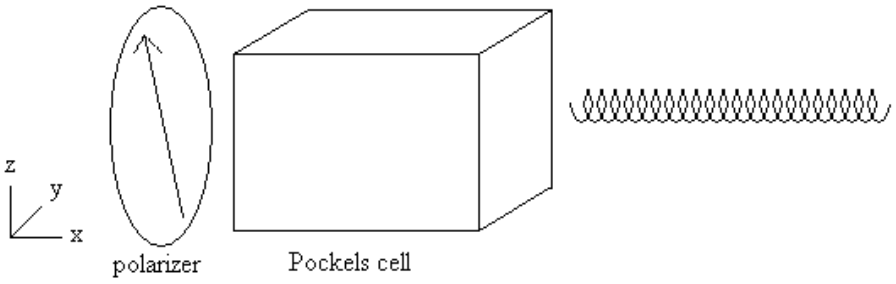

Figure 2.5: Light exits with varying polarization angle

Since the polarization angle of the light is changing with time, adding a second polarizer after the Pockels cell (Fig. 2.6) will cause the intensity of the light of the light to change with time in accordance with Malus's Law, producing amplitude modulation (9).

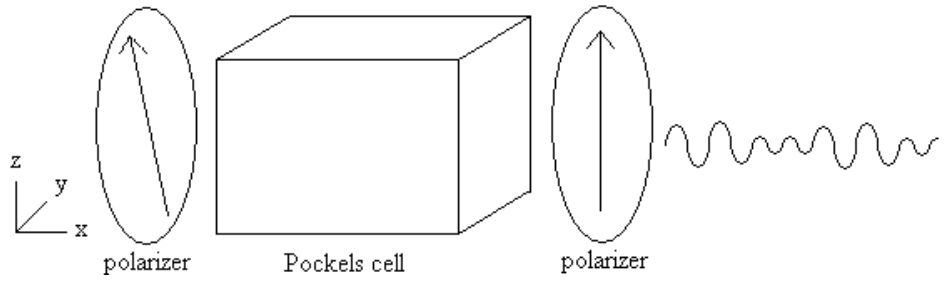

Figure 2.6: Light exits with modulated amplitude

2.4 Experimental Verification

According to the operating manual of the Pockels cell used in this experiment, a New Focus Model 4004 Broadband Phase Modulator, our particular model requires a voltage of 210V to retard the beam by π radians along the z-axis (10). Using this value for the applied voltage and equation 2.10, the height to path length ratio of the Pockels cell was found to be

$$\frac{d}{\ell} = \frac{n_e^3 r_{33} V}{\lambda} = 6.5 \tag{2.12}$$

Using this value and equation 2.11, the voltage required to produce a phase lag of π radians between the z and y axes (like a half-wave plate) was found. This required voltage, V_π, was calculated to be

$$V_\pi = \frac{\lambda d}{\ell}(n_e^3 r_{33} - n_o^3 r_{13})^{-1} = 324V \tag{2.13}$$

Having calculated the half-wave voltage, the expected signal for a given voltage across the Pockels cell was determined. Using Malus's law and equations 2.11 and 2.13, the ratio of output intensity to the incident intensity was found to be

$$\frac{I_o}{I_i} = \sin^2\left[\left(\frac{\pi}{2}\right)\frac{V}{V_\pi} + \phi\right] \tag{2.14}$$

when the first and second polarizers are aligned at 90 degrees with each other, with ϕ as the effective offset.

In order to verify this relationship, equation 2.14 was used to measure the V_π value experimentally. Both the modulated output intensity and the steady input intensity were measured for a set applied voltage, and the resulting V_π value was then calculated from equation 2.14. This experiment was repeated multiple times for both red and infrared light, and was also repeated with the polarizers set around the z and x axes of the Pockels cell (Table 2.1).

Date/time 2006	Laser Wavelength (nm)	V_π for z-axis (V)	V_π for x-axis (V)
3/1 @ 9:08	1064 (IR)	260	144
3/1 @ 10:38	1064 (IR)	140	127
3/1 @ 14:02	1064 (IR)	314	164
2/22 @ 8:05	633 (red)	174	170
2/22 @ 10:50	633 (red)	174	245
2/22 @ 13:55	633 (red)	133	140

Table 2.1: Table of V_π measurements at various times and frequencies

The expected V_π values for measurements of infrared light was 324V, and the expected value for red light was 193V (10). However, as shown in Table 2.1, not only did the measured values not correspond with the expected values, they also fluctuated wildly with respect to each other. No discernable pattern was found in how the V_π value changed from one measurement to the next. Such fluctuation could be due to impurities in the crystal coupled with the translational movement of the beam, or possibly thermal effects due to random temperature changes, but the exact cause is unknown. This experiment demonstrates that the exact output of the Pockels cell is unstable, which indicates a further need for proper feedback control.

Having found how a Pockels cell can produce either phase or amplitude modulation, the next step is to find a way to eliminate the latter while keeping the former. An ideal solution would be to simply remove all polarizers after the Pockels cell, as it is the addition of a second polarizer that causes the amplitude modulation. Unfortunately, several components in LIGO, such as mirrors, have special coatings which are sensitive to polarization. These coatings then act as a second polarizer, and regrettably they cannot be removed. Thus a feedback control system must be developed to lock the polarization angle and thus eliminate the amplitude modulation entirely. The next chapter will examine the properties of such a feedback control system.

Chapter 3: The Error Signal Generator

3.1. Basic Design of the Feedback Control Systems

Because a Pockels cell produces amplitude modulation when misaligned with the first polarizer, the most likely cause of the amplitude modulation in LIGO is that the orientation of either the polarizer or the Pockels cell slowly drifts with time. As the alignment between the first polarizer, the Pockels cell, and the subsequent polarizing elements of LIGO deteriorates, the amplitude modulation increases (11).

Thus in order to correct for the misalignment in polarization, a feedback control system must be created that will adjust the alignment automatically. Feedback control systems consist of three basic parts: an input signal generator, an error signal generator, and an actuator (12). For the Pockels cell's feedback control system (Fig. 3.1), the input generator will be a photodiode reading the output of the system after the second polarizer. The error signal generator will then isolate the signal pertaining to the misalignment, and filter out any signals in the frequency range that would interfere with LIGO's normal operation. The error signal produced will then be directed to the actuator, which will physically adjust the alignment and thus automatically eliminate the amplitude modulation. The actuator used will be discussed in the next chapter.

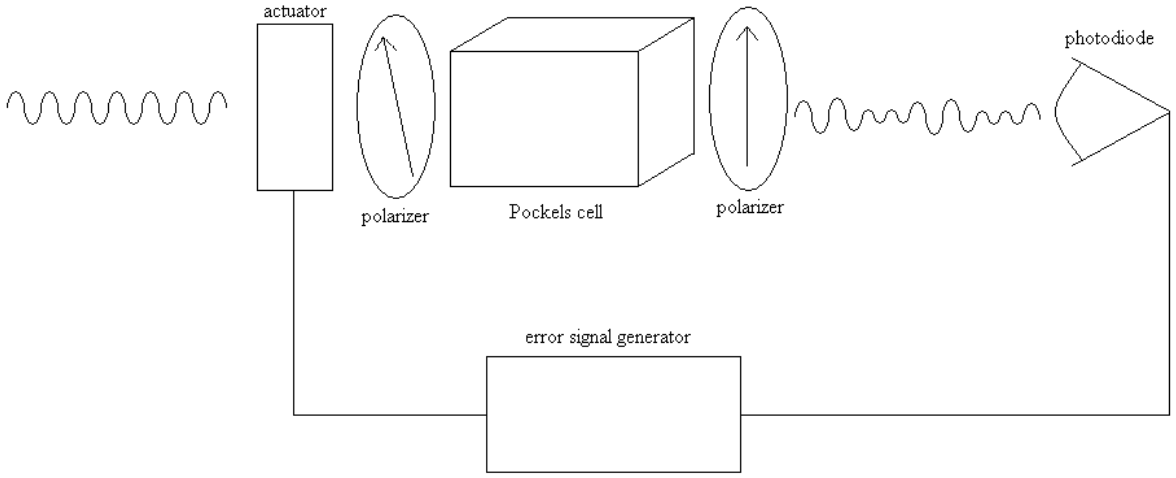

Figure 3.1: General feedback control system design

3.2 Error Signal Generator: Mixer

The error signal generator consists of two main components: an attenuator and a mixer. A mixer is an integrated circuit that multiplies two voltage signals together; in this case, the output signal from the photodiode and the voltage signal applied to the Pockels cell (Fig. 3.2).

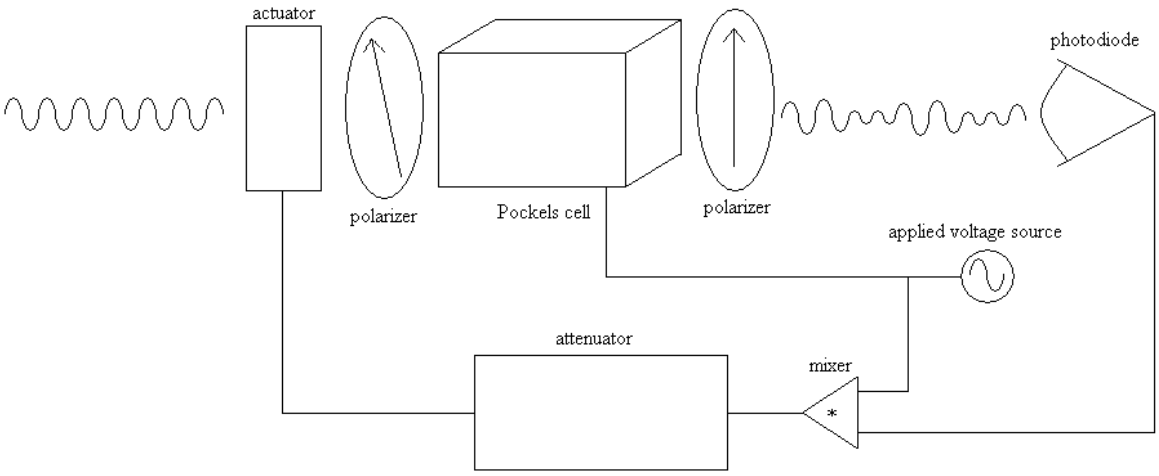

Figure 3.2: Mixer component of the feedback control system

The amplitude modulation produced from the misalignment occurs at the same frequency as the phase modulation, with the amplitude changing very slowly over time. Thus the signal for the amplitude modulation read by the photodiode (V_p) can be modeled by the equation:

$$V_p = kB\cos(\omega t) \tag{3.1}$$

where B and ω represent the amplitude and frequency of the signal directed to the Pockels cell, respectively, and k represents the function of the changing amplitude as the misalignment increases. This function consists of a combination of cosine functions at very low frequencies, but for our purposes we can approximate k to be

$$k = A\cos(\omega_a t) \tag{3.2}$$

where A and ω_a represent the magnitude and frequency of the change in amplitude over time ($\omega_a << \omega$). Thus the voltage measured by the photodiode will be the beat signal between these two functions, given by

$$V_p = AB\cos(\omega_a t)\cos(\omega t) = \frac{AB}{2}[\cos((\omega - \omega_a)t) + \cos((\omega + \omega_a)t)] \tag{3.3}$$

When this signal read by the photodiode is multiplied by the signal directed to the Pockels cell via the mixer, we find the resulting signal (V_m) to be

$$V_m = \frac{AB^2}{2}[2\cos(\omega_a t) + \cos((2\omega - \omega_a)t) + \cos((2\omega + \omega_a)t)] \tag{3.4}$$

Therefore the signal leaving the mixer is a combination of three signals, one of which corresponds solely to the increasing misalignment in polarization. Since the frequency of

that signal is much lower than the two other frequencies, it can be isolated by directing the output of the mixer through a low-pass attenuator circuit which will filter out the other two signals.

3.3 Error Signal Processor: Attenuator

In addition to isolating the low-frequency error signal that corresponds to the misalignment, the attenuator must also filter out any signals that could interfere with LIGO's normal operation. LIGO is expected to be sensitive to gravitational waves with frequencies between 40 and 1000 Hz; therefore all signals within this band must be filtered out, because actuating at these frequencies will look like a gravitational wave. In order to prevent actuation in this band, and filter out the higher-frequency signals from the mixer, the attenuator circuit needs to pass signals well below 40 Hz with a large gain, and then stop for all signals above that specified threshold.

A useful tool for analyzing a circuit's frequency response is the Bode diagram, which plots the gain of a circuit in decibels versus frequency on a logarithmic scale. For the Bode diagram, a decibel is defined as

$$1dB = 20\log a \tag{3.5}$$

where a is the gain of the circuit's transfer function. Thus the Bode diagram of a circuit in decibels is given by

$$20\log|G(j\omega)| \tag{3.6}$$

where G is the complex transfer function of the circuit with respect to frequency ω (12).

The attenuator circuit consists of two op-amps connected in series, with capacitors added to give the circuit a frequency dependence. The first op-amp (Fig. 3.3) acts as an inverting amplifier, whose gain normally has no dependence on frequency. The addition of the capacitor gives the inverting amplifier a transfer function given by equation 3.7.

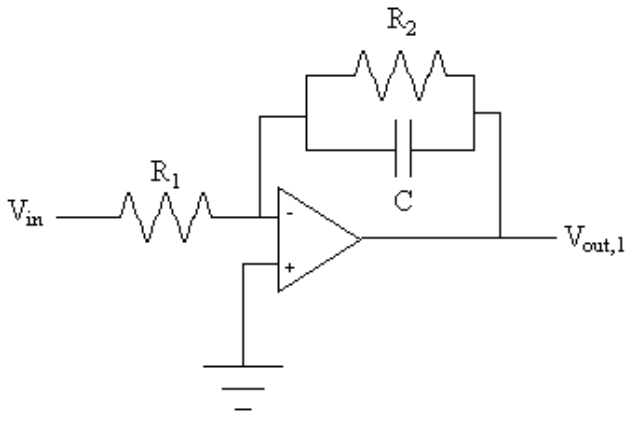

Figure 3.3: First op-amp in attenuator

$$G_1 = \frac{V_{out,1}}{V_{in}} = -\frac{R_2}{R_1(1+R_2\omega C)} \tag{3.7}$$

Thus if ω is small, the circuit passes signals with a gain of $-R_2/R_1$, and as ω increases the gain gradually goes to zero. The Bode plot of this transfer function demonstrates that the gain rolls off to zero quickly for frequencies above $(R_2C)^{-1}$, so we say that there is a "pole" at that frequency for this

circuit. However, the feedback control system requires a sharp decrease to zero for frequencies above the pole. In order to make the gain roll off more quickly, a second op-amp is needed to produce the sudden decrease to zero at the pole. Thus a second op-amp (Fig. 3.4) is added with a transfer function of

$$G_2 = \frac{V_{out}}{V_{in,2}} = -\frac{R_3(1 + R_2\omega C) + R_2}{R_3(1 + R_2\omega C)} \quad \textbf{(3.8)}$$

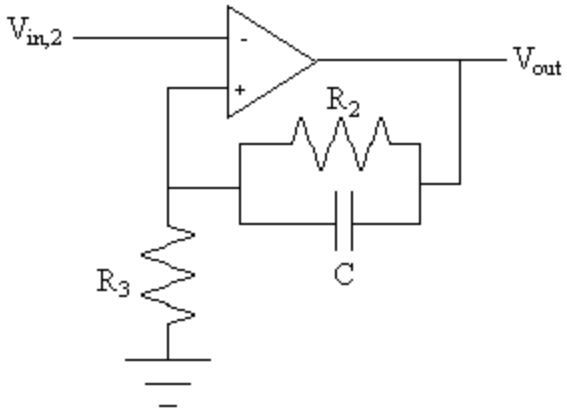

Figure 3.4: Second op-amp in attenuator

after the first op-amp. Because the input of the second op-amp is the output of the first ($V_{in,2} = V_{out,1}$), the entire attenuator circuit (Fig. 3.5) will then possess a transfer function given by

$$G = \frac{V_{out}}{V_{in}} = \frac{R_2[R_3(1 + R_2\omega C) + R_2]}{R_3R_1(1 + R_2\omega C)^2} \quad \textbf{(3.9)}$$

The Bode diagram of this transfer function (Fig. 3.6) reveals that the attenuator circuit quickly goes to zero for frequencies above the pole at $(R_2C)^{-1}$, and operates below the pole with a gain given by

$$G = \frac{R_2(R_3 + R_2)}{R_3R_1} \quad \textbf{(3.10)}$$

Both the cut-off frequency and the gain below it can be set by selecting particular values for the resistors and capacitors. For our experiments, R_1 was set at 10 kΩ, R_2 at 100 kΩ, R_3 at 5 kΩ, and C at 1 mF, which puts the cut-off frequency at 0.1 Hz and the gain below it at 60 dB.

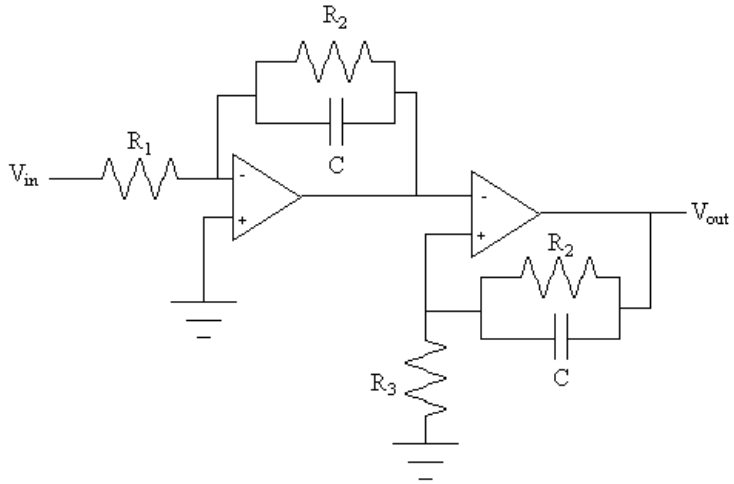

3.5: Complete attenuator circuit

Another consideration for feedback control systems is whether or not the error signal is in phase with the input signal. When the two signals are out of phase, positive feedback can occur. If the error signal reaches the actuator 180° out of phase

with the input signal, this will produce the inverse of the desired correction and thus force the Pockels cell and polarizers into further misalignment. In order to verify that such positive feedback will not occur in the desired frequency range, a Bode phase plot was taken, which plots the phase angle between the real and imaginary parts of the transfer function G($j\omega$) versus frequency on a logarithmic scale (Fig. 3.7). Because the phase angle never approaches -180^{o} for frequencies below the pole at $(R_2C)^{-1}$, the attenuator output is in phase with the input signal and thus no positive feedback should occur (12). Having filtered out the appropriate frequencies and isolated the signal corresponding to the misalignment, the error signal is then sent to an actuator. The next chapter will discuss two different actuators that were tested for this feedback control system.

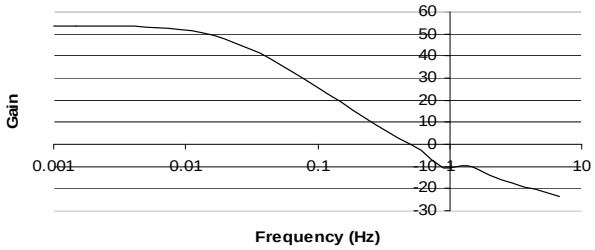

Figure 3.6: Bode diagram for attenuator (logarithmic scale)

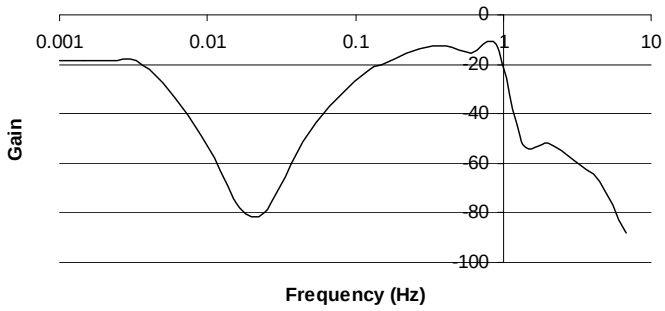

Figure 3.7: Phase diagram for attenuator (logarithmic scale)

Chapter 4: Actuators

4.1 Two Possible Actuators

Once an error signal that is proportional to the misalignment between the polarizers and Pockels cell has been generated, it is then directed to an actuator which will physically correct for the problem. Two possible actuators were considered: a Faraday rotator and a picomotor driver module. Before determining which actuator would be most effective in the feedback control system, both were examined separately.

4.2 Faraday Rotator

A Faraday rotator consists of a solenoid wrapped around a transparent dielectric material. When linearly polarized light is transmitted through the material, its angle of polarization rotates according to the equation

$$\beta = \upsilon B d \tag{4.1}$$

where β is the rotation angle, B is the magnetic field produced by the solenoid, d is the length of propagation through the dielectric material, and υ is the Verdet coefficient, an intrinsic property of the dielectric material (13). When a Faraday rotator is placed between two linear polarizers at angle θ with each other (Fig. 4.1), and the Faraday rotator produces no magnetic field, the intensity measured after the second polarizer by the photodiode is given by the Malus Law:

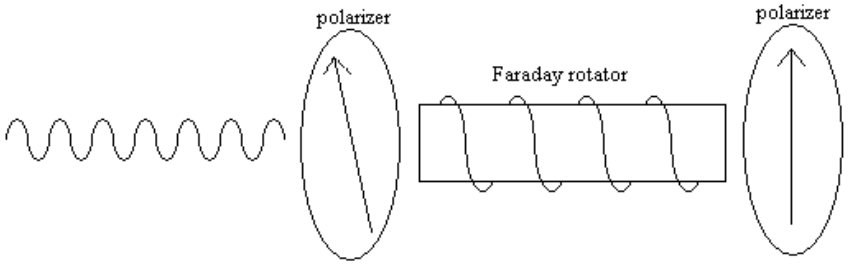

Figure 4.1: Faraday rotator

$$I = I_o \cos^2 \theta \tag{4.2}$$

However, when an AC magnetic field is produced by the coils of the Faraday rotator, the angle θ will be modulated by a small amount corresponding to β(t). The fractional modulation of the intensity is then given by

$$\frac{dI}{I}(t) = -2(\tan\theta)\beta(t) \tag{4.3}$$

and the absolute modulation scales as

$$\mathrm{dI} \propto \sin(2\theta) = \sin(\theta)\cos(\theta) \tag{4.4}$$

which will be maximized at $\theta = 45^{o}$. Because the voltage read by the photodiode is proportional to the intensity, the voltage will be modulated according to dV/V=dI/I. Substituting this relationship, and using the long solenoid approximation for the magnetic field B, we find that the modulation read by the photodiode will be given by

$$\frac{dV}{V} = -2\upsilon d\mu_{o} ni \qquad \textbf{(4.5)}$$

where i is the current applied to the Faraday rotator, and n is the number of turns per unit length of the solenoid.

Having produced this relationship, equation 4.5 was then tested by measuring the Verdet coefficient of the Faraday rotator experimentally and comparing it to the value given by the manufacturer for both red and infrared light. There were approximately 241 turns in the Faraday rotator used, with a length of 9.7 cm, and 182 mA of current was applied. While the measured values for the Verdet coefficients (Table 4.1) did not correspond with the given values for the TG20 glass that was ordered, they did correspond with the given values of another type of glass sold by the manufacturer, TGL20, indicating that they could have sent the wrong glass by mistake (13). Even so, the slightly different Verdet coefficient will not have that great an effect on the feedback control system as a whole.

Type of Light	Expected υ TG20 (arcmin/gauss-cm)	Expected υ TGL20 (arcmin/gauss-cm)	Measured υ (arcmin/gauss/cm)
Infrared	-0.075	-0.050	-0.036 +/- 0.002
Red	-2.358	-0.149	-0.156 +/- 0.006

Table 4.1: Table of Verdet coefficient measurements

In the feedback control system, the Faraday rotator is placed between the first polarizer and the Pockels cell (Fig. 4.2). The error signal is directed to the Faraday rotator, so that the resulting change in the polarization angle caused by the Faraday rotator puts the polarization angle and the Pockels cell back into alignment, thus theoretically correcting the unwanted amplitude modulation.

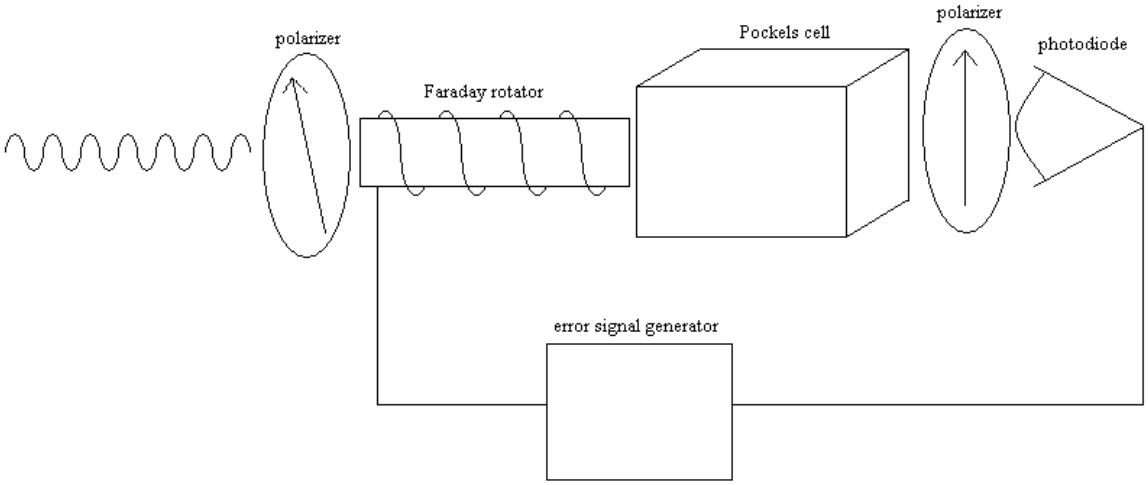

Figure 4.2: Faraday rotator within the feedback control system

4.3 Picomotor

The other actuator considered in for the feedback control system was a picomotor-driven 4-axis kinematic base attached to the base of the Pockels cell, capable of making minute adjustments to the Pockels cell's orientation. The New Focus Model 8702 PCB Mountable Single Axis Driver selected for our feedback control system is capable of rotating the separate ends of the Pockels cell about the z and x axes. Thus by placing the Pockels cell at 90^{o} with the picomotor, a positive voltage signal on the A axis would rotate it one way and a positive voltage signal on the B axis would rotate it the opposite way. In this way the picomotor will adjust the Pockels cell's orientation with the polarization angle (Fig. 4.3), and can thus be used to correct for misalignment (15).

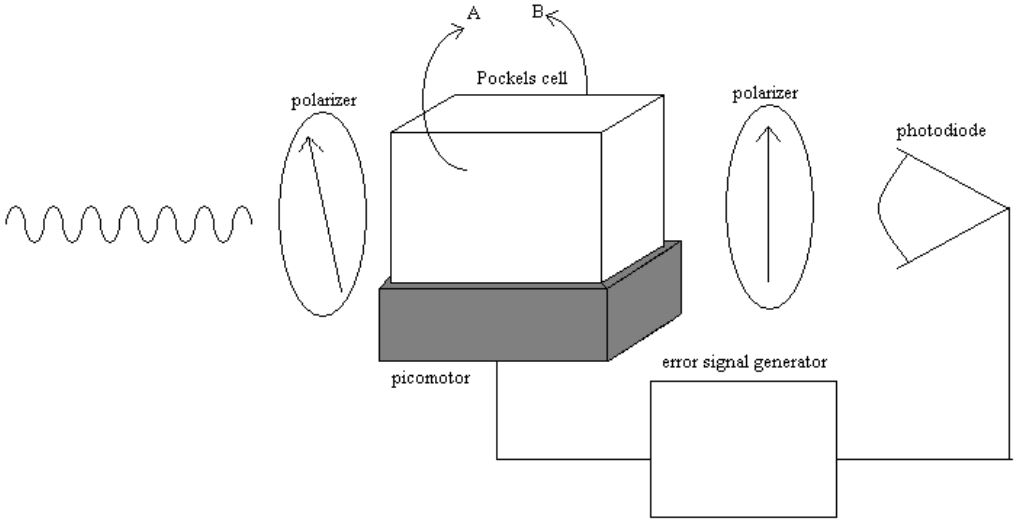

Figure 4.3: Picomotor attached to the Pockels cell's base within feedback control system

According to its specifications, the picomotor operates by sending voltage pulses to the various axes, with each pulse causing the picomotor to move approximately 0.02 μm

(15). When operating in linear voltage input mode, the pulse rate increases with every 78 mV past 1V, for both positive and negative voltages. Between +/- 1mV there is a deadband to reject noise (Fig. 4.4). This behavior was also observed by the picomotor experimentally (Fig. 4.5), within 0.1V for a given pulse rate. Thus by directing the error signal to the picomotor, the picomotor will then rotate the orientation of the Pockels cell until the error signal goes to zero and the alignment is corrected.

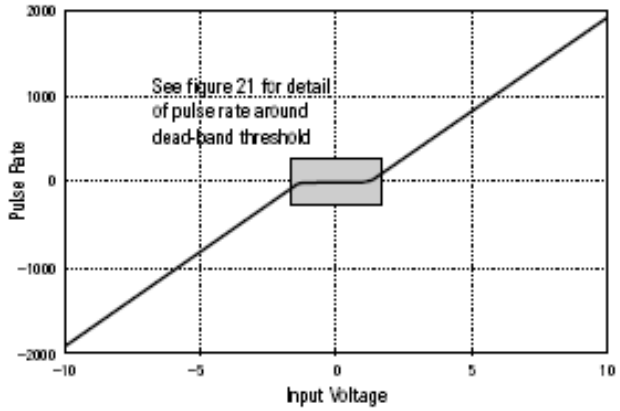

Figure 4.4: Expected picomotor behavior (15)

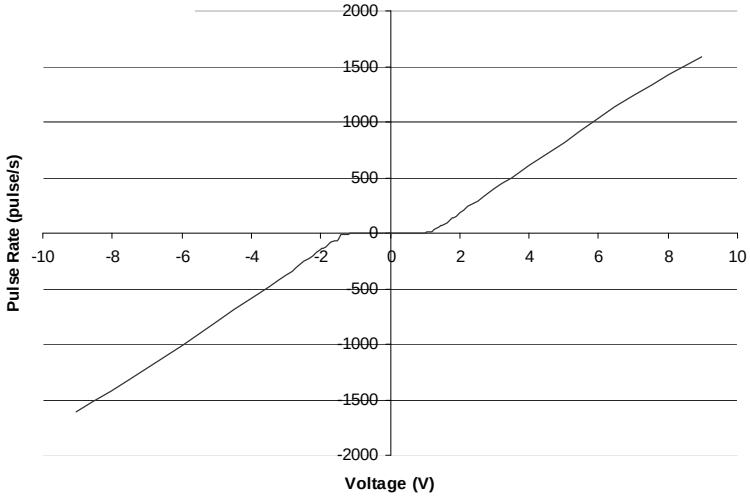

Figure 4.5: Measured picomotor behavior

Chapter 5: Experimental Performance

5.1 Experimental Set-up

Having produced the error signal generator circuit, both the Faraday rotator, and the kinematic base, the final step was to test both actuators independently and determine which would be best suited for correcting the amplitude modulation in LIGO. In order to measure how effectively the feedback control system worked, amplitude modulation was manually induced by rotating the second polarizer to test the Faraday rotator, and manually rotating the base of the Pockels cell to test the picomotor. The results from these experiments should indicate the appropriate choice of actuator when a similar feedback control system is installed at LIGO.

5.2 Faraday Rotator Performance

When testing the Faraday rotator, amplitude modulation was induced by rotating the first polarizer, producing a 20mV modulation with the same frequency as the applied voltage used to drive the Pockels cell. The Faraday rotator was then connected to the feedback control circuit, and the error signal was applied to the rotator first in one direction and then the other. For both directions, there was no measurable effect on the output modulation.

To determine if the error signal was transmitting properly, the amount of current flowing to the Faraday rotator at the maximum error signal of 15 V was measured. The result of this measurement, 20 mA, was much less than expected, and so in order to increase the current flowing to the Faraday rotator a controlled voltage source transistor circuit was added to the error signal generator after the attenuator circuit (Fig. 5.1). The transistors increased the current flowing to the Faraday rotator to 150 mA (the resistors had to be replaced with 2 W ceramic resistors to prevent overheating). However, even with this increased error signal, there was no measurable effect on output modulation in either polarity.

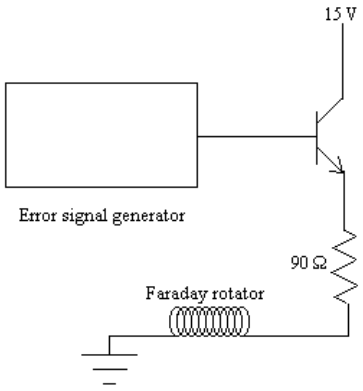

Figure 5.1: Transistor added to error signal generator

Because the modulation was induced merely by rotating the first polarizer, a Faraday rotator should be able to rotate it back and correct the alignment. This particular Faraday rotator built for this experiment was unsuccessful because it was incapable of rotating the polarization sufficiently. Manually rotating the first polarizer by a degree produced a noticeable effect, but it was determined that at maximum current the Faraday rotator used in this experiment would only be able to rotate the polarization by 0.007^{o}. Given such a limitation, the Faraday rotator proved unable to properly actuate the system.

5.3 Picomotor Performance

When testing the picomotor's performance, amplitude modulation was induced by manually tilting the Pockels cell along the B axis, creating a misalignment between the first polarizer and the Pockels cell. Tilting the Pockels cell back the other way reduced the amplitude modulation back to zero, and then caused the amplitude modulation to increase again as it passed the point of alignment.

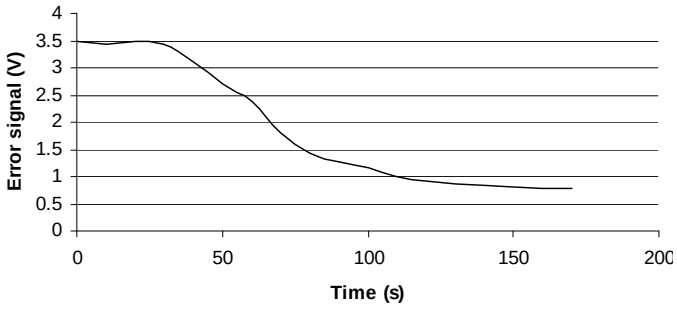

Figure 5.2: Performance of picomotor as actuator

Once the picomotor was connected to the feedback control system, the amplitude modulation induced by manually tilting the Pockels cell was reduced to less than one volt in a matter of minutes. The feedback control system also proved able to correct amplitude modulation induced by tilting the Pockels cell in the opposite direction, verifying that the system will effectively correct for amplitude modulation. Thus, unlike the Faraday rotator, the picomotor proved to be a successful actuator for this feedback control system.

Chapter 6: Conclusions

Over time, an electro-optic modulator used in a subsystem of LIGO gradually began to produce amplitude modulation. This amplitude modulation mimics the effects of a gravitational wave, and thus needed to be eliminated so that the modulation would not be mistaken for an actual signal. Believing that the source of the amplitude modulation came from a misalignment between the orientation of the polarizer and the z-axis of the Pockels cell, a feedback control system was designed to correct for any such misalignment. This feedback control system was then tested using two possible actuators: a Faraday rotator, and a picomotor kinematic base attached to the Pockels cell.

In the course of our examinations, we found that the Faraday rotator built for this experiment could not rotate the polarization enough to properly actuate the system. Any Pockels cell used to actuate the Pockels cell in LIGO would need to rotate the polarization angle on the order of a degree. For a Faraday rotator with the same Verdet coefficient to do so, either the current delivered to the Faraday rotator would need to be increased to around 27A, or the number of loops in the solenoid would need to be increased to around 36,078. Perhaps a combination of more current and loops would produce a practical Faraday rotator, but both options are limited by the amount of current that can be safely applied without overheating, and the already crowded space on LIGO's laser table. Thus using a Faraday rotator as an actuator in LIGO's feedback control system may not be feasible.

Our experiments with the picomotor, on the other hand, proved successful. For LIGO to use a picomotor to actuate the Pockels cell, it would require opposite error signals sent to the A and B axes of the kinematic base for maximum and fastest rotation. Such a system would be easier to implement than a Faraday rotator, and our experiments already indicate that such a system would be effective. Thus, having designed a feedback control system that can correct for amplitude modulation in an electro-optic modulator, this design can now be adapted for use in LIGO, bringing it one step closer to its ultimate goal of detecting gravitational waves.

References

(1) C. Will. Physics Today. Vol. 52 (10), p38. (1999)

(2) A. Abramovici, et. al. Science. 256, p325. (1992)

(3) B. Barish, R.Weiss. Physics Today. Vol. 52 (10), p44. (1999)

(4) http://www.ligo.caltech.edu/LIGO_web/other_gw/gw_projects.html

(5) http://www.ligo.caltech.edu/LIGO_web/about/ifo_diagram_big.gif

(6) P. Hariharan. Optical Interferometry. Academic Press Australia, Sydney (1985)

(7) B. Abbott, et al. Nucl. Instrum. & Methods. A517, 154 (2004)

(8) Personal communication with Dr. Dennis Ugolini regarding the contents of the LLO electronic log (dugolini@trinity.edu)

(9) A. Yariv. Optical Electronics (3rd Ed.).College Publishing, New York (1985)

(10) http://www.newfocus.com/manuals/400X_Manual_RevD.pdf

(11) S. Kawamura, M. Zucker. Applied Optics. Vol. 33 (18). (1994)

(12) C. Phillips, R. Harbor. Feedback Control Systems. Prentice Hall Inc, Englewood Cliffs (1988)

(13) F. Perdotti, P. Bandetti. American Journal of Physics. Vol. 58 (6), p542. (1990)

(14) http://www.laserglass.com.cn/english-page/index/product/Faraday.htm

(15) http://www.newfocus.com/manuals/870X_Manual_RevC.pdf